LBNL-39267
UC-000
Preprint

ERNEST ORLANDO LAWRENCE
BERKELEY NATIONAL LABORATORY

Detailed Characterization of the 1087 MeV/nucleon ^{56}Fe Beam Used for Radiobiology at the AGS

C. Zeitlin, L. Heilbronn, and J. Miller

Life Sciences Division

June 1997

Submitted to
Radiation Research

LBNL-39267
UC-000

Detailed Characterization of the 1087 MeV/nucleon ^{56}Fe Beam Used for Radiobiology at the AGS

C. Zeitlin, L. Heilbronn, and J. Miller

Life Sciences Division
Ernest Orlando Lawrence Berkeley National Laboratory
University of California
Berkeley, California 94720

June 1997

This work was supported by the NASA Space Radiation Health Program under NASA Grant L14230C through the U.S. Department of Energy under Contract No. DE-AC03-76SF00098.

Detailed Characterization of the 1087 MeV/nucleon ^{56}Fe Beam Used for Radiobiology at the AGS

C. Zeitlin, L. Heilbronn, J. Miller
Lawrence Berkeley National Laboratory, Berkeley, California 94720

Zeitlin, C., Heilbronn, L., Miller, J., Detailed Characterization of the 1087 MeV/nucleon ^{56}Fe Beam Used for Radiobiology at the AGS. *Radiat. Res.*

We report beam characterization and dosimetric measurements made using a ^{56}Fe beam extracted from the Brookhaven National Laboratory Alternating Gradient Synchrotron with a kinetic energy of 1087 MeV/nucleon. The measurements reveal that the depth-dose distribution of this beam differs significantly from that obtained with a 600 MeV/nucleon iron beam used in several earlier radiobiology experiments at the Lawrence Berkeley Laboratory's BEVALAC. We present detailed measurements of beam parameters relevant for radiobiology, including track- and dose-averaged LET, fragment composition, and LET spectra measured behind sample holders used in biology irradiations. We also report measurements of fluence behind three depths (1.94, 4.68, and 9.35 g cm^{-2}) of polyethylene targets with the 1087 MeV/nucleon beam, and behind 1.94 g cm^{-2} of polyethylene with a 610 MeV/nucleon beam delivered by the AGS. These results are compared to earlier measurements with the 600 MeV/nucleon beam at the BEVALAC.

INTRODUCTION

It has been recognized for many years that irradiation by high-energy heavy ions in the Galactic Cosmic Rays (GCR) may affect the health of humans on long-duration spaceflight both inside and outside the geomagnetosphere (1). Because iron ions are the most densely ionizing particles which are present in significant numbers in the GCR, there has been considerable interest in understanding their transport through matter and their biological effects. Accordingly, numerous radiobiology experiments using iron ions were conducted at the Lawrence Berkeley Laboratory's BEVALAC, with typical extracted beam energies of 400 to 600 MeV/nucleon. After the shutdown of the BEVALAC in early 1993 (with the last radiobiology experiments in December 1992), there was no facility in the U.S. for radiobiology experiments with high energy heavy ions until October 1995, when a 1087 MeV/nucleon (at extraction) iron beam became available for radiobiological use at the Brookhaven National Laboratory's Alternating Gradient Synchrotron (AGS). A beamline modeled on one used for similar irradiations at the BEVALAC was constructed at the AGS, and a dosimetry system incorporating many elements of the BEVALAC system was implemented. Several radiobiology experiments and one physics experiment were performed on this beamline in 1995; additional measurements were performed in October 1996. At the end of the 1996 run, a 610 MeV/nucleon ^{56}Fe beam was extracted from the AGS and transported to the experimental area, with the primary purpose of establishing that such a beam could be reliably delivered. Some physics measurements and biology irradiations were performed with this beam as well.

In this paper, we focus primarily on some properties of the 1087 MeV/nucleon AGS iron beam which are important for the interpretation of the biology experiments. (Throughout, Linear Energy Transfer in water — formally, LET_∞ — is abbreviated to LET.) We present beam characterization data consisting of measurements of: beam energy; fluence vs. LET as seen at the upstream edge of a biological sample; dose vs. LET; track- and dose-averaged LET (2) measured behind several sample holders used in biology irradiations; radial beam uniformity; and the Bragg curve. We also present fluences behind polyethylene targets, and compare them to similar fluences measured at the BEVALAC.

MATERIALS AND METHODS

Dosimetry System

Measurements of the physical characteristics of the AGS iron beams were performed with two separate systems. The conventional dosimetry system consisted of three parallel-plate ionization chambers (IC1, IC2 and IC3), used in conjunction with a variable-depth water column. The IC's were used to monitor the dose received by biological samples, and when the desired dose was achieved, to provide a beam cutoff signal to the accelerator. Each IC has two gas volumes; in the upstream

volume, ionization electrons are collected on a foil divided into quadrants, while in the downstream volume, they are collected on a foil that consists of a series of concentric rings. The real-time readout from the quadrants is used along with information from in-beam multi-wire proportional counters to adjust the beam position; the readout of the rings provides pulse-to-pulse monitoring of the uniformity of the radial dose distribution. (Higher resolution uniformity monitoring is done by means of x-ray films placed in the beam and read out off-line.) An additional function of the IC's is the measurement of the Bragg curve, which is obtained by taking the ratio of charge collected in a chamber placed downstream of the water column (IC3) to the charge collected in a chamber upstream of the column (IC1), as a function of depth of water. This ratio gives a characteristic peak when the water column depth is near the nominal range of the beam particles.

Silicon Detector System

A stack of silicon detectors, used primarily for fragmentation measurements (3), was used for several beam characterization measurements as well. This system was previously used at the BEVALAC (4,5). The arrangement of the detectors on the beamline for the 1995 run is shown in Figure 1a; this setup was designed for cross section measurements and was not optimized for beam characterization. For a portion of the 1996 run, the detector setup was altered specifically for beam characterization; this configuration is shown in Fig. 1b. In the 1995 data-taking, the trigger required a coincidence of particles in T1 and T2, with thresholds set so that the trigger did not fire if the incident particle had an LET below about 20 keV/μm. For measuring cross sections, which are determined by normalizing to the number of incident iron ions, this threshold is much lower than necessary; however, for beam characterization, the threshold cut-off is a deficiency. The trigger in 1996 was defined by a coincidence of hits in d3mm1 and d3mm2 with the thresholds set much lower, so that incident particles over the entire LET range were detected.

In silicon detectors of the type used here, each trigger causes a readout of the deposited energy, or ΔE, in each detector. This quantity is proportional to the sum of the square of the charges of the particles that hit the detector, i.e., the detectors measure an effective charge $Z_{eff}^2 = \sum_i Z_i^2$ on each event. (This approximation is good as long as the particles all have similar velocities.) If only a single particle is present, as was the case for the majority of events reported here, there is no complication. Also, if the charge of one particle (*e.g.*, a heavy fragment with charge close to that of the primary iron) is much greater than that of any other particles present, the heavy fragment dominates the effective charge, even if the lighter particles are at somewhat lower velocity than the heaviest particle.

For a given particle type and velocity, the ratio between LET and ΔE/Δx in silicon is mildly energy-dependent. For present purposes, this ratio is well-approximated by a constant, which varies by less than 0.5% over the entire range of particles encountered in the experiment, from the 1087 MeV/nucleon iron to 200 MeV protons. Thus, in the data presented below, the LET scale is determined by multiplying the measured ΔE in silicon detectors by factors which cause the iron peaks to appear at 148 keV/μm. The factors are determined separately for the setups shown in Fig. 1a and 1b, using data taken with no sample holders on the beamline. (That is, there is one scale factor which applies to all the 1995 data, and another for all of the 1996 data.)

Measurements Behind Polyethylene Targets

Polyethylene is a convenient tissue equivalent material, both because of its chemical composition (CH_2) and its ease of handling. Data taken behind these targets can be combined with data taken behind pure carbon targets to extract fragment production cross sections in hydrogen targets, as in Ref. (3). For present purposes, measurements behind polyethylene also yield insight into the tissue-equivalent depth-dose distribution (since polyethylene is so similar to water), illustrate the nature of the mixed radiation fields seen at depth in tissue, and allow for comparisons to model calculations.

Table I summarizes the data collected behind polyethylene targets at the BEVALAC and AGS. The configuration of the detectors on the beamline at the BEVALAC made it difficult to determine the proper normalization, and only a single low-statistics run was taken with no target. These "target-out" data are needed for background subtraction. In contrast, the configurations used at the AGS (Figs. 1a for data sets C, E and F, and 1c for data set B) make normalization trivial by identifying the incident particle, so that off-line analysis cuts can guarantee that a single iron particle triggered the event; also, high-statistics target-out runs were taken. Further, identification of particle species in the AGS data was more straightforward than in the BEVALAC data.[1]

Corrections for Background

We limit these data samples to events in which a single iron particle is incident on the target. Ideally, under this condition, data taken without a target would yield spectra consisting of 100% iron and nothing else in the downstream detectors. But due to materials on the beamline and imperfections in the data analysis methods, this is not the case and corrections to the spectra measured behind targets must be applied. The corrected fluence of iron particles seen behind a target is given by:

$$\phi_{Fe}(\text{corrected}) = \phi_{Fe}(\text{observed})/\phi_{Fe}(\text{target - out})$$

and for fragments of charge Z:

$$\phi_Z(\text{corrected}) = \phi_Z(\text{observed}) - \phi_Z(\text{target - out})\phi_{Fe}(\text{corrected})$$

The corrected fluence of iron particles is related to the mean free path λ by

$$\lambda = \frac{-x}{\log(\phi_{Fe}(\text{corrected}))}$$

where x is the target depth.

Corrections for Unequal Target Depths

The corrected fragment yields defined above sum to $1 - \phi_{Fe}(\text{corrected})$, since (effectively) one particle is detected

per event. For a small variation in areal density of the target (ρx), it is approximately true that, for a given Z, $\phi_Z \rightarrow \phi_Z + \delta\phi_Z$ where

$$\frac{\delta\phi_Z}{\phi_Z} = \frac{\delta(1-\phi_{Fe})}{(1-\phi_{Fe})}$$

We make use of these relationships to adjust the 1.82 and 4.55 g cm^{-2} fluences so that they are equivalent to the 1.94 and 4.68 g cm^{-2} fluences, respectively.

Corrections for Acceptance

Because the d3mm detectors used for particle identification in data sets A, B and D had small acceptance, the measured fluences must be corrected; we use Goldhaber's statistical model of fragmentation (6, 7) to calculate angular distributions and hence acceptance as a function of Z, beam energy, and angle subtended by the detectors. The results for those data sets have been corrected according to this model. Data sets C and E were obtained with a larger acceptance (3.5°), and no corrections are needed (i.e., the model predicts 100% acceptance) for the $Z \geq 12$ fluences presented here.

RESULTS

Measurements of Beam Energy - 1995

The nominal energy of the beam at AGS extraction was 1087 MeV/nucleon. The beam traversed several materials before entering the experimental area through a thin exit window which marked the end of the vacuum line. (In the following, we refer to the point just downstream of this final window as "at the exit window.") The Bragg curve for 1995, shown in Fig. 2, has a peak in the ionization ratio at 27.8-27.9 cm of water, depending on which ring is considered. In interpreting the location of the peak, it is necessary to account for the entrance and exit windows on the water column, which in total consist of 1.63 g cm^{-2} of water-equivalent acrylic. Also, the beam traversed approximately 2 meters of air, or about 0.24 g cm^{-2}, before reaching the water column entrance window. Thus the true range of the beam was approximately 29.7 cm of water, which, according to standard range-energy tables (8), corresponds to a beam energy of about 1060 MeV/nucleon at the exit window. In a separate calculation[2], we have used a heavy ion transport model (10, 11) to simulate the passage of an iron particle through the materials between the point of extraction from the AGS and the exit window in the experimental area. For an extraction energy of 1087 MeV/nucleon, this calculation predicts an energy of 1064 MeV/nucleon, in excellent agreement with the energy determined from the Bragg peak.

An independent measurement of beam energy was made using silicon detectors d3mm1, 2, 3 and 4. Pulse heights were converted into measurements of deposited energy, ΔE, using a standard calibration scheme (see Ref. (4) for details). We define the following quantity for each of the d3mm detectors:

$$\text{Ratio}(i^{th}\text{ detector}) = \frac{\Delta E_i(\text{Iron peak, target in})}{\Delta E_i(\text{Iron peak, target out})}$$

where the peaks were found by selecting events which passed tight cuts to insure that the entire detector stack was traversed by a single iron ion. The resulting histogram for each detector was then fit with a Gaussian distribution to the central bins. Calculations with our transport model show that, with a thick target, the ratios are very sensitive to the energy of the beam at the exit window. Data taken behind a 10.4 cm polyethylene target are in excellent agreement with the calculation using a beam energy of 1087 MeV/nucleon at extraction, which implies an energy of 1064 MeV/nucleon at the exit window and 1055 MeV/nucleon at the biology sample position. Varying the extraction energy in the calculation — or varying the list of materials upstream of the exit window — yields ratios which do not agree with the data.

The two methods yield results that are mutually consistent, and show that iron ions at the exit window have an LET of 147.8 keV/μm. Calculations show that after traversing 2 meters of air and the 3 ionization chambers — to reach the typical biological sample location — the LET of iron ions is 148.1 keV/μm.

Measurements of Beam Energy - 1996

The Bragg curve data for 1996 have a peak in the ionization ratio at 27.4 cm of water, about 5 mm less than was found in the 1995 data. Taking into account the additional materials on the beam line, this corresponds to a range in water of 29.2 cm. From Ref. (8), we find that this range corresponds to a kinetic energy of 1053 MeV/nucleon, about 7 MeV/nucleon lower than was found by this method in the 1995 data. The difference is attributable to the presence of beam-monitoring detectors upstream of the vacuum exit window which were taken out during the 1995 run but which were in the beamline during the 1996 run. Calculations show that the slightly lower beam energy has a negligible effect on the LET for iron particles, which remains very close to 148 keV/μm.

The beam energy measurement using the ratio of ΔE's in silicon detectors was repeated with 1996 data. Again, the results favor an extraction energy of 1087 MeV/nucleon, which in turn leads to a predicted energy of 1058 MeV/nucleon at the exit window, 6 MeV/nucleon lower than was found by this method in the 1995 data. This value is in excellent agreement with that determined from the Bragg curve.

Fluence and Dose vs. LET

Since the 1995 data were subject to a 20 keV/μm trigger threshold, we use the 1996 data to determine fluence[3] (ϕ), dose and integrated dose, all as functions of LET, for the beam at the exit window. Both years' data are used to determine these same quantities behind sample holders; corrections for the trigger threshold effects are made to the earlier data.

Fluence vs. LET

Figure 3a shows ϕ vs. LET obtained by taking the sum of deposited energies in d3mm1 and d3mm2, with data obtained in 1996. The spectrum corresponds closely to what would be seen at the upstream edge of a sample holder. Two cuts were applied to the data to obtain this spectrum: they require that the same particle hit each detector (and traversed both intact), and that the ΔE in each was significantly above zero. Energy-loss calculations show that a beam-velocity proton will deposit approximately 1.3 MeV in a detector of 3 mm thickness; since this is the lowest plausible ΔE for a valid beam particle in this experiment, we set the low-end cuts in the pulse-height spectra to correspond to 1.0 MeV in d3mm1 and d3mm2.

In Fig. 3a, a very large peak of iron events stands out, even with a logarithmic scale on the vertical axis. The events with ΔE below the iron peak are presumably fragments created when an iron ion interacts in material upstream in the beamline; lighter ions produced in the accelerator which survive transport to the experimental area also populate this region. The track-averaged LET is 112 keV/μm; this value is strongly influenced by the peak at low LET, and is sensitive at the level of about ±3% to details of the cuts used to define the data sample. The dose-averaged LET is found to be 145 keV/μm, and this quantity is much less sensitive to details of the cuts.[4]

Dose vs. LET

The fluence spectrum shown in Fig. 3a was used to generate a plot of dose (in arbitrary units) as a function of LET, by multiplying the fluence in each bin by the value of LET at the center of the bin and entering the product into a new histogram, which was then normalized to have an integral of 1. The result is shown in Figure 3b. Clearly, although there is a large peak in the fluence spectrum at low LET, those particles do not contribute much to the dose. This point is further illustrated in Fig. 3c, in which the integral of Fig. 3b (again normalized to 1) is shown as a function of LET. Less than 3% of the dose is attributable to particles with LET < 100 keV/μm, and another 3% is attributable to particles with 100 < LET < 140 keV/μm; the remaining 94% of the dose is contributed by iron particles.

Dose- and Track-Averaged LETs Behind Sample Holders

We are interested in fluences and doses measured behind sample holders used in radiobiology experiments on the AGS beamline. Some of these data were collected in 1995, others in 1996. To correct for particles below the trigger threshold in the 1995 data, we use LET < 20 keV/μm data obtained in the 1996 run, which show that 23% of the total number of tracks were in this region (with an average LET of 3 keV/μm). Accordingly, for each sample holder for which we took data in 1995, the ϕ vs. LET spectrum was normalized so that its integral was 0.77, and the low-LET fluence spectrum was then added to the measured spectrum. The resulting spectrum is then used for calculations of all quantities of interest. (These same quantities were calculated directly from the 1996 ϕ vs. LET spectra with no corrections.)

Fluences were measured behind several sample holders used in the biology experiments. In the 1996 run, holders were placed on the beamline upstream of d3mm1 (see Fig. 1b); in the 1995 run, they were placed in the target position indicated in Fig. 1a. In Table II, we list track- and dose-averaged LETs, percentage of dose contributed by iron particles, and percentage of dose from particles with LET > 100 keV/μm.

Figure 4 shows a typical ϕ vs. LET spectrum obtained behind a sample holder, in this case a single polystyrene flask filled with cell-culture medium. (Results for this holder are reported in the third row from the top of Table II). Due to the energy loss in the flask, the energy of the surviving iron ions is slightly reduced, causing the LET peak to shift from 148 keV/μm to about 150 keV/μm. Several peaks, corresponding to ion species lighter than iron, are plainly visible in the histogram; the peak for manganese (Z = 25) is at about 139 keV/μm, on top of the low-end tail of the iron distribution from which

it is barely distinguishable. Other peaks are visible down to Z = 12. We note that there is a slight preference for the production of even-Z nuclei, as can be seen from the (generally) higher peaks for those species compared to neighboring odd-Z nuclei. A similar trend is seen in other iron fragmentation data (3,5), including data presented below.

Beam Uniformity

In order to insure a uniform dose distribution over the entire sample surface, the radial and quadrantal dose distributions were monitored during the irradiations, using the segmented ionization chambers. As was the case at the BEVALAC, the AGS beam transport system is optimized for a beam diameter on the order of 1 cm, which must be enlarged to several cm in order to irradiate most biological samples. The way this is done at the AGS is different from the approach used at the BEVALAC. There, some defocusing of the beam was done using upstream magnets before the beam was finally transported through a set of thin lead scattering foils. At the AGS, all beam defocusing is done using upstream beamline magnets, which results in a coupling of the beam steering and beam profile.

Two distinct beam tunes were used for the biology experiments during the 1995 and 1996 runs at the AGS, referred to as low dose-rate (1-2 Gy per minute in 1995, 0.5 Gy per minute in 1996) and high dose-rate (8-10 Gy per minute in 1995, 12-15 Gy per minute in 1996) modes. Table III shows typical dose distributions for both modes of running for IC3, which was closest to the samples and thus was the primary dose and dose distribution monitoring device. The radial distributions for rings 1 through 7 are shown, with the outer diameter of the ring indicated in parentheses in the first column. The dose distributions for typical 1995 low-dose rate and high-dose rate runs are shown in the second and third columns, and the values for typical 1996 runs are shown in the fourth and fifth columns. Because most of the biological sample holders were no larger than 6 cm in any dimension, the dose distributions were optimized for uniformity on the four innermost rings. Over those rings, the dose in 1995 low dose-rate runs (column two) varied by ±2-3% relative to the average dose. The 1996 low dose-rate runs showed slightly higher values in the variation over the first four rings. For the high dose-rate runs (columns three and five), the dose varied by ±4-7%, with little difference between the 1995 and 1996 runs. Because defocusing is the sole technique for spreading out the beam, in general some dose uniformity must be sacrificed at the highest dose rates. Table III shows that the low dose-rate runs have a slightly smaller variation in the dose uniformity than do the high dose-rate runs.

In addition to the radial distributions, the quadrant foil of IC3 was used to extract the "top to bottom" and "east to west" ratios. Those ratios are shown in the last two rows of Table III, labeled "T/B" and "E/W", respectively. The T/B ratio is calculated by subtracting the sum of the bottom two quadrants from the sum of the top two quadrants, and then dividing that difference by the sum of all four quadrants. The E/W ratio is calculated by subtracting the sum of the two beam-right quadrants from the sum of the two beam-left quadrants, and dividing that difference by the sum of all four quadrants. The T/B and E/W ratios varied from run to run, but the values shown in the table are typical of low dose-rate and high dose-rate runs. The dependence of areal dose distribution on the mode of operation that is observed in the radial distributions is not reflected in the T/B and E/W ratios.

Interpretation of the Bragg Curve

The difference between the Bragg curves obtained at 1087 MeV/nucleon and 600 MeV/nucleon is illustrated in the inset in Fig. 2, which covers the full range of water column depth used for the 600 MeV/nucleon beam. We note that over the first 4 cm of water, there is little difference; at greater depths, the difference becomes quite pronounced, with the ratio rising for the lower-energy beam and falling for the higher-energy beam. Also, the ionization ratio peaks at about 4 for the 600 MeV/nucleon beam, as opposed to approximately 1 for the 1087 MeV/nucleon beam.

There is a straightforward explanation for the differences between these depth/dose curves. As shown in Ref. (5), for a 600 MeV/nucleon beam and polyethylene targets, the track-averaged LET was nearly constant over the range of target depths from 0 to 5 cm, due to the offsetting effects of fragmentation and energy loss. Fragmentation produces ions lighter than iron and hence with lower LET, whereas the velocity lost in traversing the target causes particles of all species to have higher LET at the exit than they did at the entrance. At 600 MeV/nucleon, the effects balanced each other almost exactly over the first 5 cm of polyethylene (4.6 g cm^{-2}). Only with an 8 cm target (7.3 g cm^{-2}) did the track-averaged LET increase, meaning that the velocity decrease was having a greater influence than the fragmentation. This explains the upturn in the Bragg curve seen at a similar depth of water. At 1087 MeV/nucleon, the energy loss curve is much flatter than it is at 600 MeV/nucleon[5], which partly explains the behavior of the Bragg curve at the AGS energy: the small increase in LET with depth is insufficient to balance the increasing fragmentation of the beam into lighter ions.

Calculations using the NUCFRG2 nuclear fragmentation model (11) show that the mean free path for fragmentation of iron in water is 10 cm; therefore at 29.7 cm (the range of the 1087 MeV/nucleon beam) only about 5% of the incident iron ions survive. In contrast, about 30% of the iron survives at 12 cm, the location of the Bragg peak for 600 MeV/nucleon. Regardless of energy, the fraction of surviving iron strongly influences the value of the ionization ratio in the peak of the Bragg curve, because the peak value is essentially an average (over a large number of particles and a wide range of LET) of the ratio for individual particles. Therefore it is not surprising that at 600 MeV/nucleon, where a substantial fraction of the incident iron survives, the peak in the Bragg curve is a factor of 4 higher than that in the 1087 MeV/nucleon curve, where very little iron survives.

The dose decreases monotonically with depth over the first 23 cm of H_2O with a 1087 MeV/nucleon beam. Over the range 1-12 cm, the Bragg curve is well fit by the quadratic expression $D(x) = 1.06 - .048x + .0012x^2$ where D is the dose relative to that at the upstream edge of the sample holder, and x is the depth in cm. The uniformity of dose across a sample thus degrades with increasing depth. For example, if a sample of 8 cm depth receives a dose of 1 Gy at the upstream edge, the dose in the center will be about 0.9 Gy and about 0.75 Gy at the downstream edge. Qualitatively speaking, the effects seen for the 1087 MeV/nucleon iron beam will be observed for any heavy ion beam of sufficient energy such that the position of the Bragg peak distance is substantially greater than the nuclear interaction mean free path. Experimenters working with thick samples and comparable beams should be aware of these effects.

Fluence Results Behind Polyethylene Targets

For $Z < 12$, the BEVALAC data suffered from inefficient triggering and the measured fluences were low by a large factor (estimated to be in the range 2-3). In all lower-energy data sets, substantial acceptance corrections are needed at low Z. And in data sets C, E and F, clear peaks in the PSD2 spectra for individual fragment species are not clear below $Z = 12$. Thus, in the following, we restrict comparisons to the range $Z \geq 12$.

600 MeV/nucleon Fluence Measurements Compared

We begin by comparing data sets taken with similar beam energies. At the BEVALAC, materials upstream of the polyethylene targets degraded the nominal 600 MeV/nucleon beam to an energy of 510 MeV/nucleon at the target entrance. Largely because no lead scattering foils were used at the AGS, the 610 MeV/nucleon extraction energy is less degraded at the target entrance, to 555 MeV/nucleon according to our calculations. The two energies are sufficiently close to make a direct comparison meaningful. After all corrections, we obtain the fluences shown in Table IV and graphically in Fig. 5a. Uncertainties in the AGS data are much smaller than in the BEVALAC data, and have been suppressed in the plot in order to facilitate the comparison. The χ^2 between the two sets is 13.2 for 12 degrees of freedom; the agreement can therefore be said to be reasonably good. This tends to validate the normalization procedures used in Ref. (5). Also, we find that the mean free path of iron ions is consistent between experiments — the BEVALAC data yield a value of 8.0 ± 0.5 g cm^{-2}, compared to 8.3 ± 0.2 g cm^{-2} at the AGS. We consider the AGS data to be more reliable, for reasons outlined above. Also shown in Fig. 5a. (as a line) are the predictions of the transport model described in Ref. (10).

600 MeV/nucleon Fluences Compared to 1087 MeV/nucleon

With the 1087 MeV/nucleon beam energy at extraction, the iron energy at the target entrance was about 1050 MeV/nucleon. Table IV and Figures 5b and c show the fluences obtained at the two beam energies.

For the thinner target, we compare AGS data sets; for the thicker, AGS data are compared to BEVALAC data. Model predictions are shown for all cases. The thin-target fluences shown in Fig. 5b vary slightly with beam energy, with more production of the heaviest fragments at the lower energy and more production of lighter fragments at the higher energy. Also at the higher energy, the mean free path for iron to undergo a nuclear interaction is 8.2 ± 0.2 g cm^{-2}, extremely close to the value obtained at the lower energy. Thus, the sum of all fragment fluences is approximately independent of energy, while the individual fragment fluences show some variations with energy.

For the thick-target fluences shown in Fig. 5c, the trend is the same, but the large error bars on the BEVALAC data preclude a definitive judgment. (The fluences for $20 \leq Z \leq 25$ are all higher at the lower energy.) At the higher energy, the mean free path for iron is found to be 8.2 ± 0.2 g cm^{-2}, at the lower energy, 7.9 ± 0.5 g cm^{-2}, again consistent with little or no energy dependence of the charge-changing nuclear cross section.

Thick-target Fluence at 1087 MeV/nucleon

A measurement behind 9.35 g cm^{-2} of polyethylene was made with the 1087 MeV/nucleon beam. Fluence results are shown in the far-right column of Table IV. Comparing these fluences to those for data set E illustrates an interesting point: the increases in fluences of heavy fragments are suppressed at large target depth compared to the increases in fluences of lighter fragments. For instance, at 9.35 g cm^{-2}, ϕ for manganese ions is only 13% higher than at 4.68 g cm^{-2}, whereas ϕ for silicon ions (Z = 14) is 76% higher with the thicker target. This effect is due to secondary, tertiary and higher-order interactions in the target: the cross sections increase with fragment mass, so that more heavy fragments interact than do light fragments. Further, these secondary and tertiary interactions tend to increase the yields of lighter fragments, since the number of heavy secondaries which interact and "feed down" to lighter fragments increases with depth. These data demonstrate the importance of multiple interactions in heavy-ion transport models.

Comparisons Between Data and Model

In Ref. (10), Fig. 5a, and Fig. 5c, for the 600 MeV/nucleon Fe beams, the model predicts a higher fluence of the heaviest fragments ($22 \leq Z \leq 25$) than is measured; the discrepancy is most pronounced for Cr (Z = 24). For the 1.94 g cm^{-2} data, the model is in good agreement with the data over the rest of the spectrum, while at 4.68 g cm^{-2}, the model predictions are generally lower than the data. The data show an enhancement in fluence for even-Z ions which is not predicted by the model. In Fig. 5b and 5c, the model predictions for the higher-energy beam are in excellent agreement with the data. These results suggest that the NUCFRG2 part of the code, which calculates the fragmentation cross sections, needs adjustment in its energy-dependent portions.

Track-Averaged LETs Behind Polyethylene in 1087 MeV/nucleon Spectra

We previously reported track-averaged LET's of 166, 162, 167 and 216 keV/μm for our BEVALAC data behind 0, 1.82, 4.55 and 7.28 g cm^{-2} of polyethylene, respectively. If we take ratios of the non-zero depth values to the zero-depth value, we obtain .98, 1.01 and 1.30. When these points are plotted with the Bragg curve (Fig. 2 inset), they fall quite near the actual Bragg curve data for this beam energy. Similarly, the 1087 MeV/nucleon AGS polyethylene data yield track-averaged LETs of 147, 135, 117 and 95 keV/μm for target-out, 1.94, 4.68 and 9.35 g cm^{-2} of polyethylene, respectively. Like the BEVALAC data, these points, too, fall quite near the Bragg curve data for this beam energy. This indicates that the dose measurements obtained with the ionization chambers are sensitive to track-averaged LET, as expected.

CONCLUSIONS

We have measured several important quantities related to 1087 MeV/nucleon ^{56}Fe beams used for radiobiology at the BNL AGS, including depth-dose distribution, and track- and dose-averaged LET of the beam at the entrance and exit of biological sample holders. Some beam characteristics are significantly different from those of the 600 MeV/nucleon energy beams used in similar experiments at the LBL BEVALAC. The respective Bragg curves show the strong effects of the interplay between ionization energy loss and nuclear fragmentation as a function of beam energy, which must be accounted for in planning biological irradiations, especially of thick samples. Fluence spectra for $12 \leq Z \leq 25$ obtained at the AGS behind polyethylene have been reported and compared to previous BEVALAC measurements, demonstrating good agreement for similar data and showing the energy dependence of the fluences. The data were also compared to a transport model and show good agreement over most of the range of fragment charge.

ACKNOWLEDGMENTS

Many individuals at LBNL and in the BNL AGS, Biology and Medical departments contributed to the success of the AGS radiobiology runs, and we particularly thank D. Lazarus and W. McGahern of the AGS staff for their outstanding technical and logistical support. We are indebted to B. Ludewigt, M. Nyman and especially R. P. Singh of LBNL for generous donations of their time and expertise with the dosimetry system. We are grateful to W. Schimmerling of the NASA Space Radiation Health Program for his long-time support and encouragement of this program. We thank T. Borak and S. Rademacher of Colorado State University, and T. Carter and C. Stronach of Virginia State University, for their help in putting the experiment together. We appreciate the assistance given by A. Kronenberg of LBNL in editing this manuscript. This work was supported at LBNL by the NASA Space Radiation Health Program under NASA Grant L14230C through the U.S. Department of Energy under Contract No. DE-AC03076SF00098.

FOOTNOTES

1. Particle identification in the AGS data is also simpler because: (1) at higher beam energies like 1087 MeV/nucleon, events due to any particular fragment species appear as a distinct Gaussian-shaped distribution, well-separated from the other fragment species; (2) with the 610 MeV/nucleon AGS beam, relatively thin targets were used so that the separation remained good; (3) improved triggering allows us to see the entire spectrum of fragments with good statistics.

2. The energy loss calculations were performed by numerical integration of the Bethe-Bloch equation (9) using an appropriately small step size. We note that at 1087 MeV/nucleon, the density effect is significant and must be taken into account. This is not the case at 600 MeV/nucleon.

3. We refer to planar fluence. In the context of the beam characterization data, unit incident fluence is a single beam particle which deposited energy in the trigger detectors (T1 and T2 in 1995, d3mm1 and d3mm2 in 1996) sufficient to fire the trigger. In the context of the measurements behind polyethylene, unit incident fluence is a single iron particle incident on the target.

4. In the 1995 data, with very few events below 20 keV/μm, the track-averaged LET is found to be 142 keV/μm, the dose-averaged LET 147 keV/μm. As a check of consistency between the 1995 and 1996 data, we calculated track- and dose-averaged LET values using the 1996 data but including only the particles with LET > 20 keV/μm; the resulting values were within 1% of those obtained with the 1995 data.

5. For an illustration, see the curves on pg. 132 of Ref. (9).

REFERENCES

1. "Guidance on Radiation Received in Space Activities", Recommendations of the National Council on Radiation Protection and Measurements. NCRP Report No. 98, Bethesda, MD (1989), and references therein.

2. "Linear Energy Transfer," ICRU Report No. 16. International Commission on Radiation Units and Measurements, Bethesda, Maryland (1970).

3. C. Zeitlin, L. Heilbronn, J. Miller, S. E. Rademacher, T. Borak, T. R. Carter, K. A. Frankel, W. Schimmerling and C. E. Stronach, Heavy fragment production cross sections from 1.05 GeV/nucleon ^{56}Fe in C, Al, Cu, Pb and CH_2 targets, *Phys. Rev. C*, in press.

4. C. Zeitlin, K. A. Frankel, W. Gong, L. Heilbronn, E. J. Lampo, R. Leres, J. Miller and W. Schimmerling, A modular solid state detector for measuring high energy heavy ion fragmentation near the beam axis, *Radiat. Meas.* **23**, 65-81 (1994).

5. C. Zeitlin, L. Heilbronn, J. Miller, L. Heilbronn, K. Frankel, W. Gong and W. Schimmerling, The fragmentation of 510 MeV/nucleon Iron-56 in polyethylene. I. Fragment fluence spectra. *Rad. Res.* **145**, 655-665 (1996).

6. A. S. Goldhaber, Statistical models of fragmentation processes, *Phys. Lett.* **53B**, 306 (1974).

7. R. K. Tripathi and L. W. Townsend, Simple parameterization of fragment reduced widths in heavy ion collisions, *Phys. Rev.* **C49**, 2237 (1994).

8. "Stopping Powers and Ranges for Protons and Alpha Particles", ICRU Report No. 49. International Commission on Radiation Units and Measurements, Bethesda, Maryland (1993).

9. Particle Data Group, "Review of Particle Properties", *Phys. Rev. D* **54**, (1996).

10. C. Zeitlin, L. Heilbronn, J. Miller, L. Heilbronn, W. Schimmerling, L. W. Townsend, R. K. Tripathi and J. W. Wilson, The fragmentation of 510 MeV/nucleon Iron-56 in polyethylene. II. Comparisons between data and a model. *Rad. Res.* **145**, 666-672 (1996).

11. J. W. Wilson, J. L. Shinn, L. W. Townsend, R. K. Tripathi, F. F. Badavi and S. Y. Chun, NUCFRG2: A semiempirical nuclear fragmentation model, *Nucl. Instr. Meth.* **B** 94, 95-102 (1994).

FIGURE CAPTIONS

1. Schematic diagrams of detector system used to make particle fluence measurements. 1a. The 1995 arrangement. 1b. The 1996 arrangement used for beam characterization studies. 1c. The 1996 configuration used for measurements behind polyethylene with the 610 MeV/nucleon beam.

2. Bragg curve for 1087 MeV/nucleon ^{56}Fe, using data from ring 1, the innermost ring in the IC's. The inset figure shows the Bragg curve obtained with a 600 MeV/nucleon beam, and the 1087 MeV/nucleon beam over the same depth of water.

3a. Fluence vs. LET of the "raw" beam (i.e., as seen at the exit window), obtained with the 1996 data. 3b. Dose vs. LET based on Fig. 3a, as described in the text. 3c. Integral of dose vs. LET. The plotted quantity is, for the i^{th} bin, $\sum_{i=1}^{L_i} D(L_i) \Big/ \sum_{j=1}^{180} D(L_j)$ where the summation runs over the bins of the histogram show in Fig. 3b.

4. Fluence vs. LET measured behind a flask filled with cell culture medium.

5. Fragment fluences behind polyethylene targets. From top to bottom, the plots show the results behind: a. 1.94 g cm^{-2} for 600 MeV/nucleon (at extraction) iron beams at the BEVALAC and at the AGS; b. 1.94 g cm^{-2} at the AGS at two beam energies; c. 4.68 g cm^{-2} for the 600 MeV/nucleon iron beams at the BEVALAC and the 1087 MeV/nucleon AGS beam. Model predictions are shown as lines.

TABLE I
Data Sets With Iron On Polyethylene

Energy at target entrance(MeV/nucleon)	Target Depth (g cm^{-2})	Year Taken	Designation	Detector Acceptance
510	1.82	1992	A	1.5°
555	1.94	1996	B	2.0°
1050	1.94	1995	C	3.5°
510	4.55	1992	D	1.5°
1050	4.68	1995	E	3.5°
1050	9.35	1995	F	3.5°
510	7.28	1992	G	1.5°

TABLE II
Track- and Dose-Averaged LETs and Fe Dose Fractions Behind Sample Holders

Sample Holder Description	$\overline{LET}_{trk}$ keV/μm (note 1)	$\overline{LET}_{dose}$ keV/μm (note 2)	% of Dose, L > 140 keV/μm	% of Dose, L > 100 keV/μm
none	112	145	94	97
Falcon T-25, 1 side	110	145	94	97
Falcon T-25, 2 sides, empty	109	145	93	97
Falcon T-25, filled	100	143	86	93
Falcon T-25, filled+ 1 side	100	143	85	93
Falcon T-75, filled	93	142	83	92
Corning 25 cm^2, 25100-25	98	143	86	93
(Corning 25 cm^2, 25100-25)×2	90	140	78	89
Corning 60-mm tissue culture dish, #25010	106	145	93	97
tapered cylindrical beaker[3], empty	108	145	93	97
cylindrical beaker[3], water-filled	86	138	74	87
Fisher 1013 petri dish, filled	109	146	93	97
(Fisher 1013 petri dish, filled)×2	107	146	91	96
(Fisher 1013 petri dish, filled)×3	104	144	88	95

Notes. 1. Track-averaged LET values have uncertainties of approximately ± 3%. 2. Dose-averaged LET values have uncertainties of approximately ± 1%. 3. Cylinder dimensions: height, 10 cm; diameter at top, 8 cm; diameter at bottom, 6.5 cm.

TABLE III

Radial and Quadrantal Dose Distributions for Both Modes of Radiobiology Runs

IC3	1995 Low Dose Rate (1-2 Gy/min)	1995 High Dose Rate (8-10 Gy/min)	1996 Low Dose Rate (0.5 Gy/min)	1996 High Dose Rate (12-15 Gy/min)
Ring 1 (1 cm)	360.4 cGy	7132 cGy	93.3 cGy	8152 cGy
Ring 2 (2 cm)	374.9 cGy	7113 cGy	93.0 cGy	7909 cGy
Ring 3 (4 cm)	366.9 cGy	6737 cGy	88.4 cGy	7748 cGy
Ring 4 (6 cm)	363.1 cGy	6470 cGy	82.0 cGy	7204 cGy
Ring 5 (8 cm)	341.5 cGy	5847 cGy	70.4 cGy	6402 cGy
Ring 6 (10 cm)	317.5 cGy	5127 cGy	57.8 cGy	5448 cGy
Ring 7 (18 cm)	135.3 cGy	2048 cGy	18.1 cGy	2015 cGy
T/B	0.044	0.074	-0.001	0.075
E/W	-0.069	-0.047	0.042	-0.008

TABLE IV

Corrected Fragment Fluences ($\times 10^3$) Behind Polyethylene Targets

Z	1.94, 510	1.94, 555	1.94, 1050	4.68, 510	4.68, 1050	9.35, 1050
25	25.0 ± 3.1	29.2 ± 0.7	25.5 ± 0.5	45.0 ± 3.6	42.8 ± 1.1	49.7 ± 1.1
24	21.7 ± 3.0	25.0 ± 0.5	20.0 ± 0.4	39.5 ± 3.0	37.3 ± 1.0	44.5 ± 1.0
23	15.7 ± 2.6	16.9 ± 0.4	15.7 ± 0.4	31.8 ± 3.0	27.7 ± 0.9	38.0 ± 0.9
22	14.6 ± 2.4	16.7 ± 0.4	15.7 ± 0.4	29.9 ± 3.0	29.6 ± 0.9	40.0 ± 0.9
21	11.7 ± 1.8	12.3 ± 0.4	12.6 ± 0.3	23.3 ± 1.8	22.5 ± 0.8	32.7 ± 0.9
20	13.0 ± 1.8	10.5 ± 0.4	11.8 ± 0.3	24.7 ± 1.9	23.3 ± 0.8	35.8 ± 0.9
19	8.0 ± 1.7	8.2 ± 0.3	8.9 ± 0.3	17.8 ± 1.9	19.0 ± 0.7	27.5 ± 0.8
18	8.0 ± 1.5	7.1 ± 0.3	9.0 ± 0.3	16.2 ± 1.5	18.5 ± 0.7	28.5 ± 0.8
17	5.7 ± 1.6	5.6 ± 0.3	7.5 ± 0.3	13.9 ± 1.7	15.6 ± 0.6	22.9 ± 0.7
16	6.5 ± 1.7	5.3 ± 0.3	7.6 ± 0.3	18.5 ± 1.8	15.9 ± 0.6	26.3 ± 0.8
15	6.1 ± 1.4	4.3 ± 0.3	5.7 ± 0.2	12.6 ± 1.5	12.3 ± 0.6	21.8 ± 0.7
14	4.3 ± 2.3	5.3 ± 0.4	7.4 ± 0.5	14.9 ± 2.5	15.8 ± 0.6	27.8 ± 0.8
13	7.1 ± 1.5	3.9 ± 0.3	5.6 ± 0.3	13.0 ± 1.5	12.4 ± 0.6	22.6 ± 0.7
12	3.1 ± 1.8	4.5 ± 0.4	5.0 ± 0.3	12.3 ± 2.8	12.9 ± 0.6	20.4 ± 0.7

Notes. Fluences are per incident Fe ion. Numbers in column headings separated by commas are target areal density in g cm^{-2} and beam energy at target entrance in MeV/nucleon. Fluences for data set G are reported in Ref. (5).

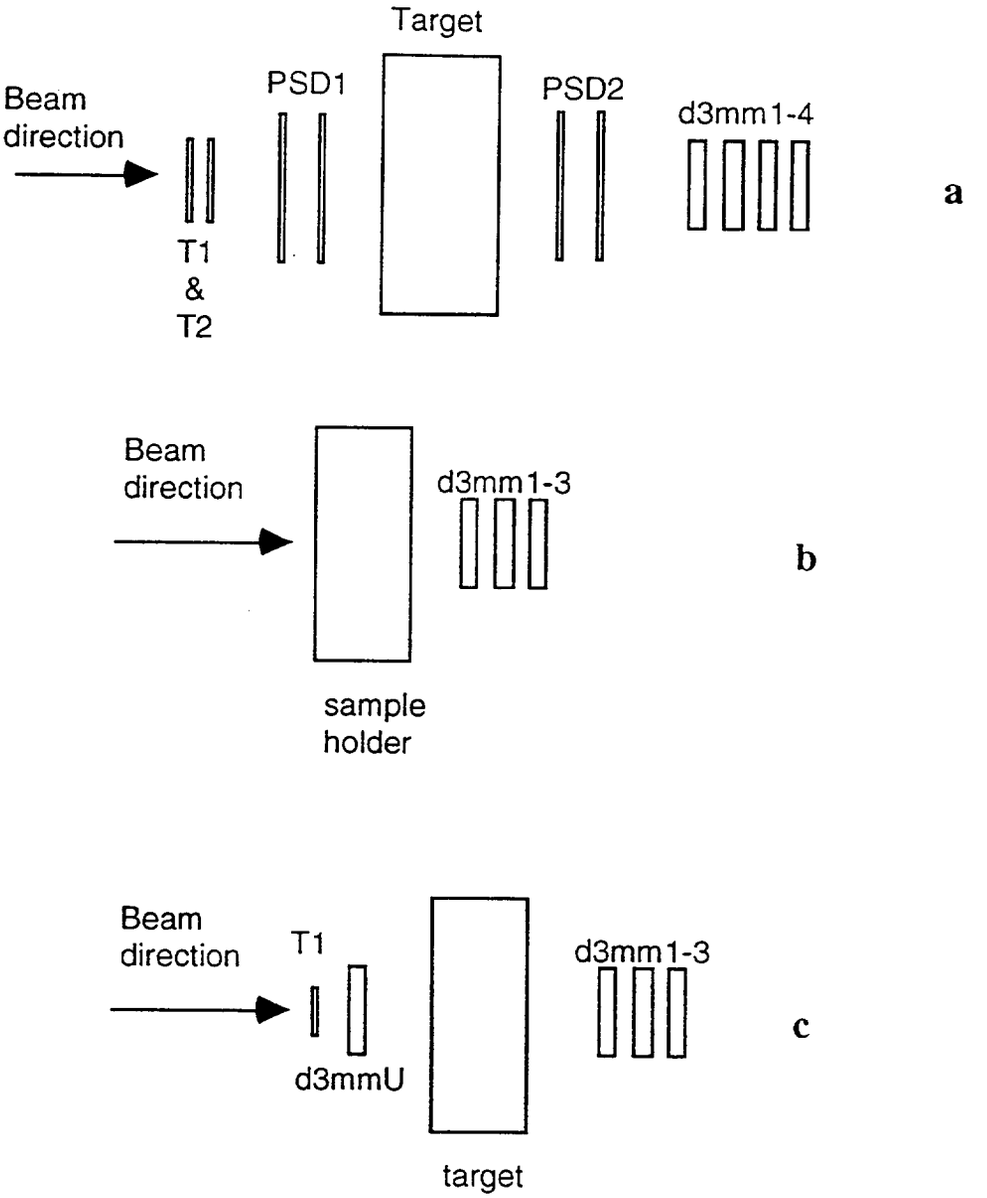
Target
Beam direction
PSD1
PSD2
d3mm1-4
T1 & T2
a
Beam direction
d3mm1-3
b
sample holder
Beam direction
T1
d3mm1-3
d3mmU
c
target

Figure 1

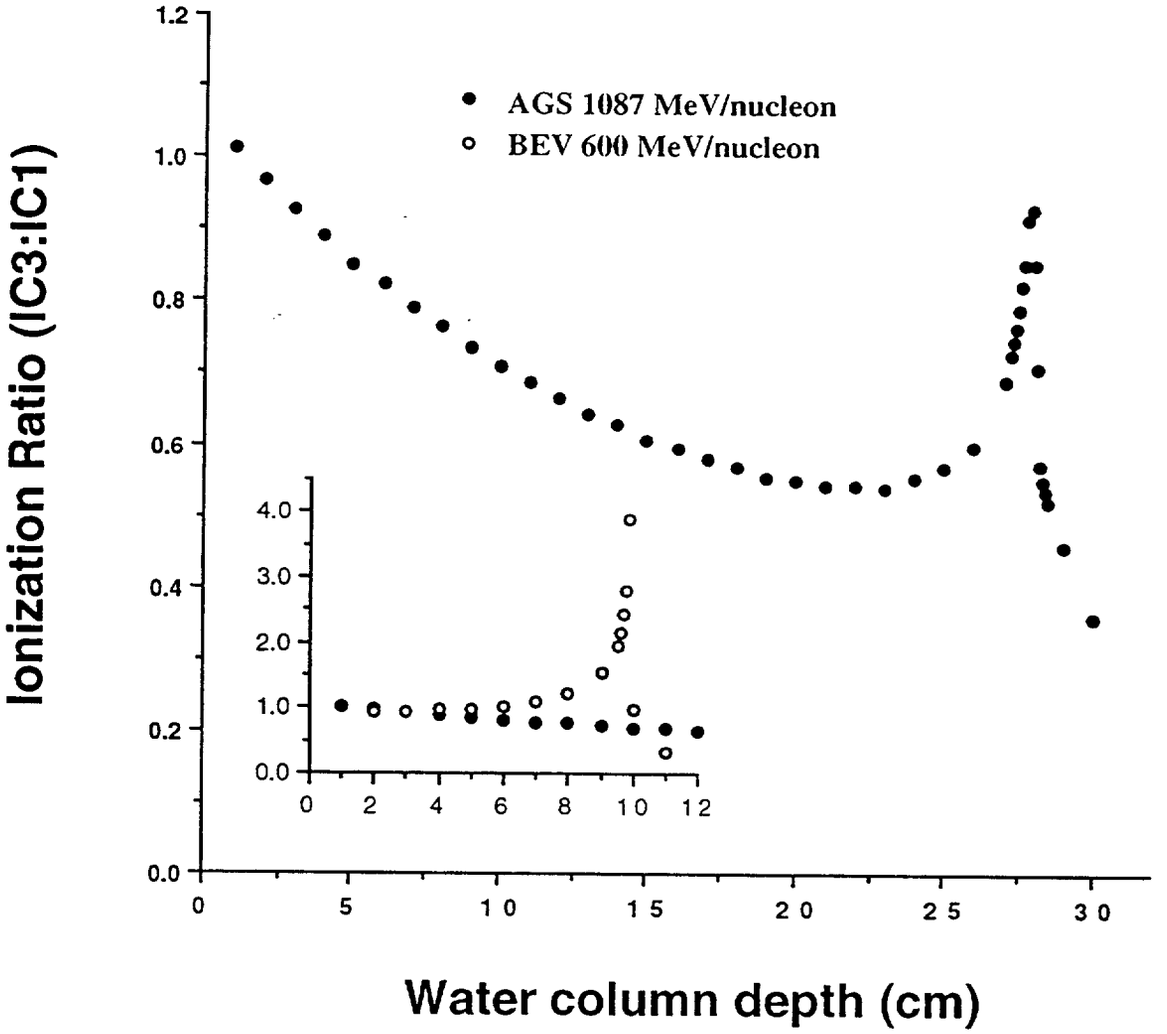
AGS 1087 MeV/nucleon
BEV 600 MeV/nucleon
Ionization Ratio (IC3:IC1)
Water column depth (cm)
1.2
1.0
0.8
0.6
0.4
0.2
0.0
0
5
10
15
20
25
30
4.0
3.0
2.0
1.0
0.0
0
2
4
6
8
10
12

Figure 2

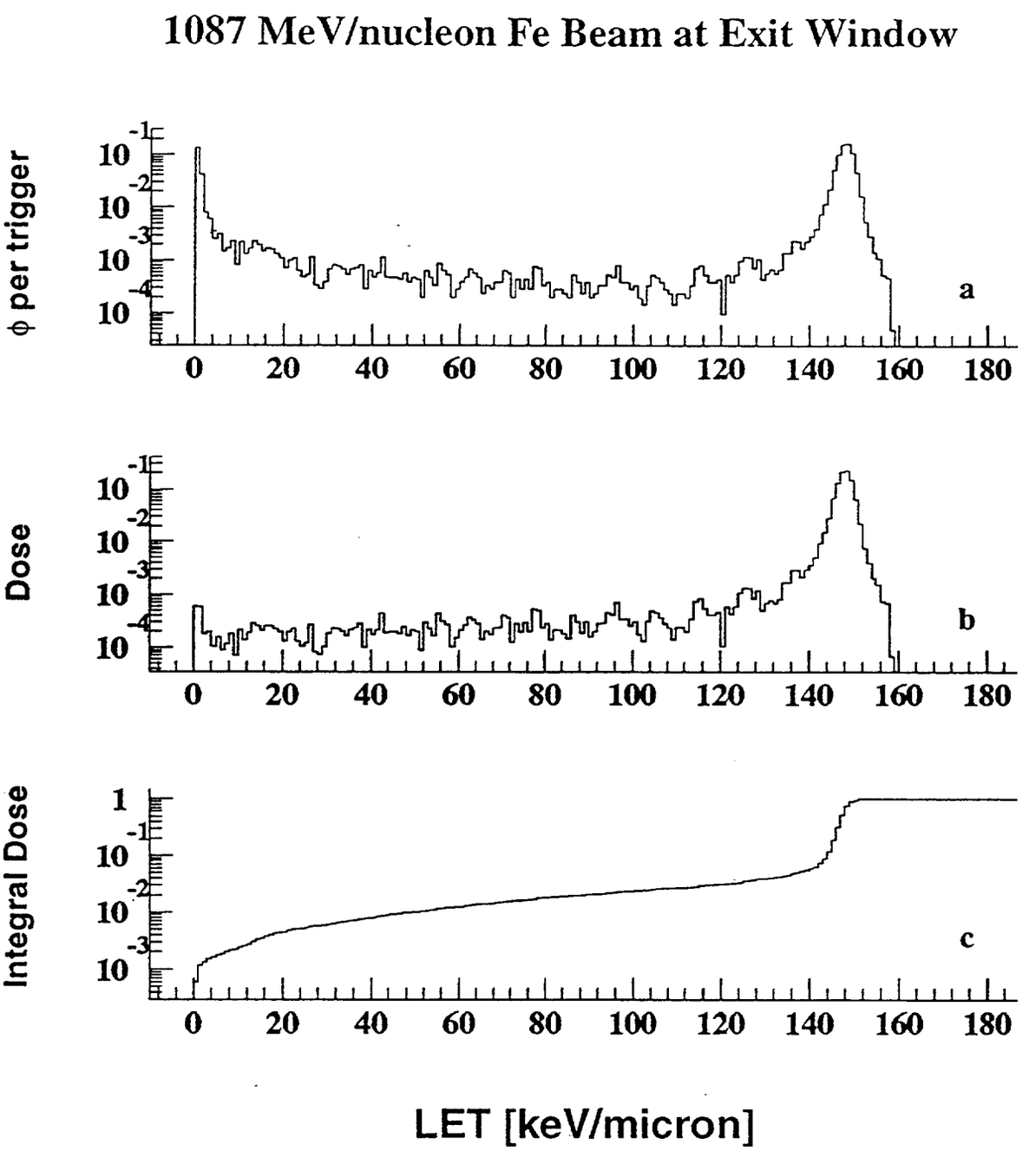
1087 MeV/nucleon Fe Beam at Exit Window
ϕ per trigger
Dose
Integral Dose
a
b
c
0
20
40
60
80
100
120
140
160
180
LET [keV/micron]

Figure 3

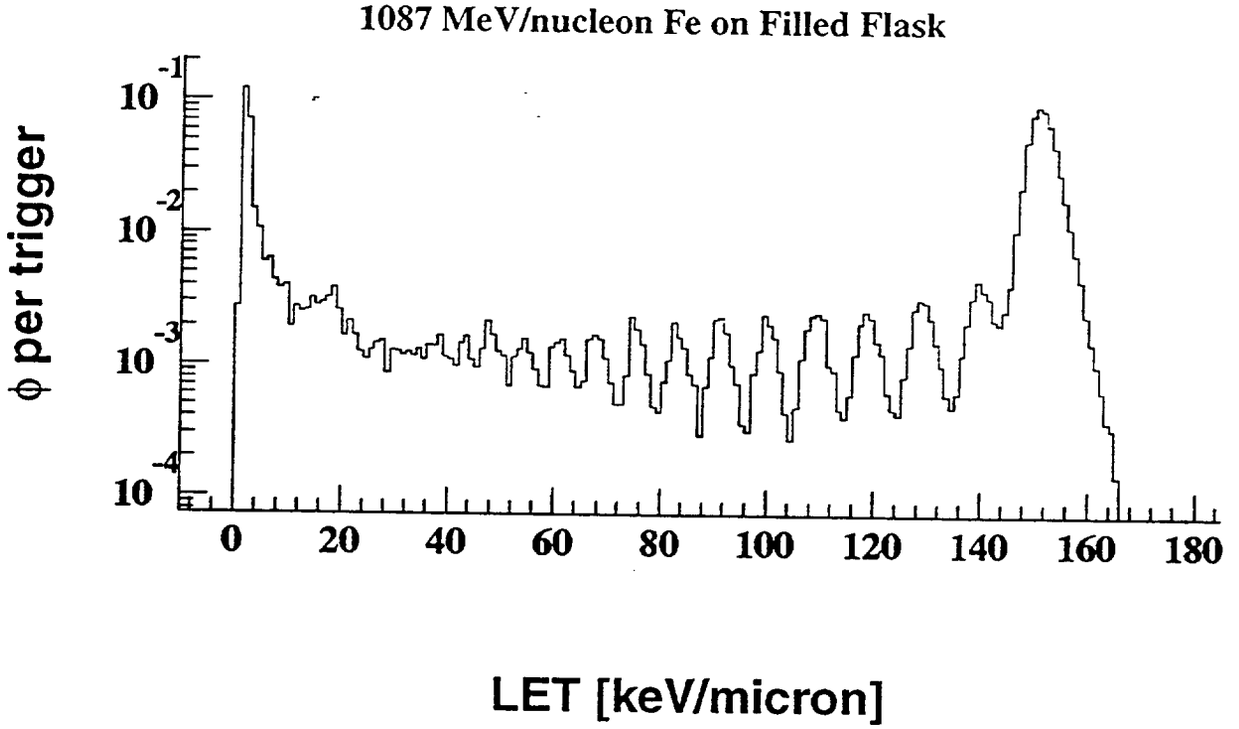
1087 MeV/nucleon Fe on Filled Flask
ϕ per trigger
10^-1
10^-2
10^-3
10^-4
0
20
40
60
80
100
120
140
160
180
LET [keV/micron]

Figure 4

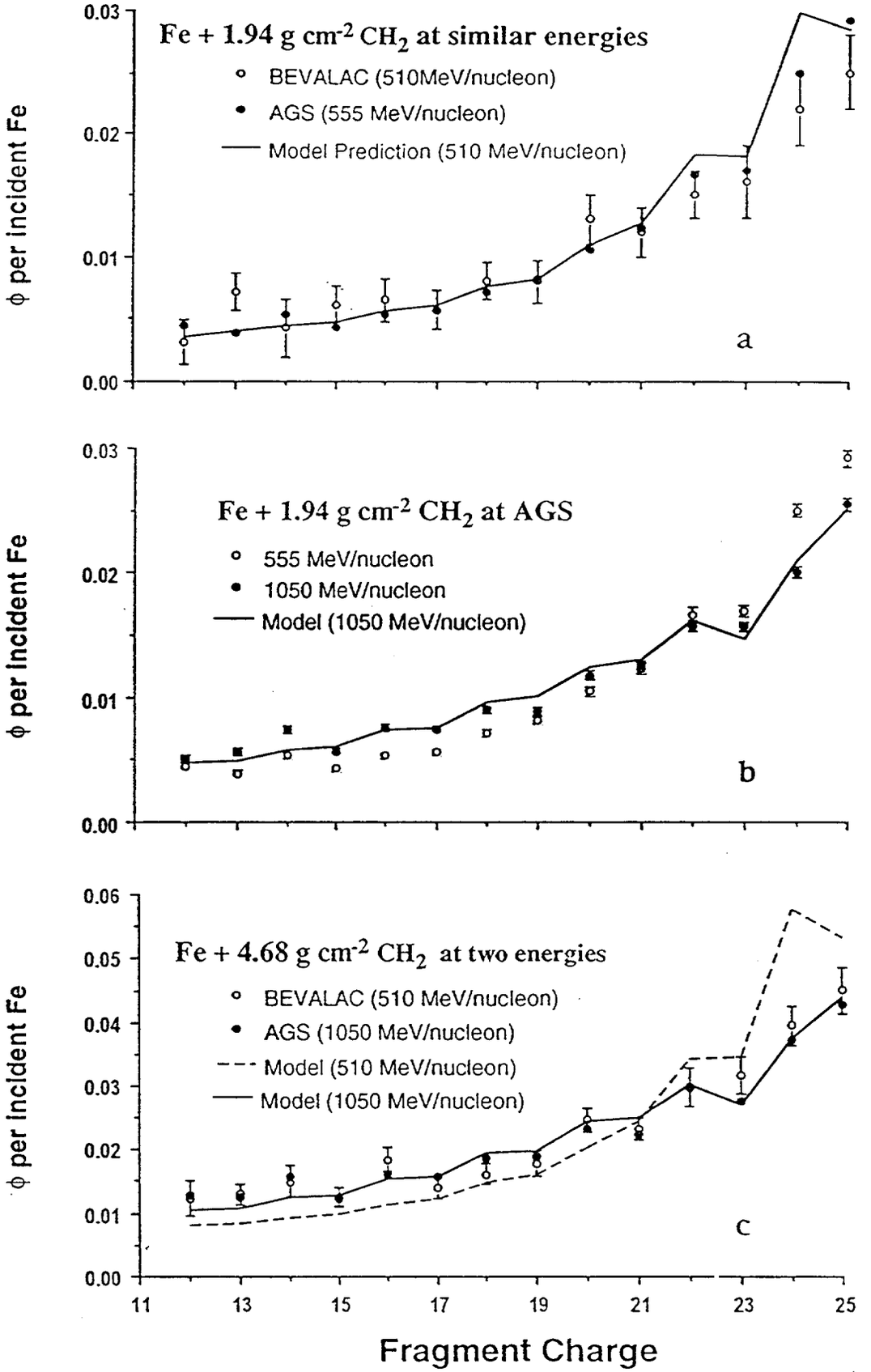
Fe + 1.94 g cm-2 CH2 at similar energies
BEVALAC (510MeV/nucleon)
AGS (555 MeV/nucleon)
Model Prediction (510 MeV/nucleon)
a
Fe + 1.94 g cm-2 CH2 at AGS
555 MeV/nucleon
1050 MeV/nucleon
Model (1050 MeV/nucleon)
b
Fe + 4.68 g cm-2 CH2 at two energies
BEVALAC (510 MeV/nucleon)
AGS (1050 MeV/nucleon)
Model (510 MeV/nucleon)
Model (1050 MeV/nucleon)
c
ϕ per Incident Fe
Fragment Charge
0.00
0.01
0.02
0.03
0.04
0.05
0.06
11
13
15
17
19
21
23
25

Figure 5